Available online at www.sciencedirect.com
SCIENCE DIRECT®
Journal of Computational Physics 212 (2006) 617–636
JOURNAL OF COMPUTATIONAL PHYSICS
www.elsevier.com/locate/jcp

Central finite volume schemes with constrained transport divergence treatment for three-dimensional ideal MHD

R. Touma [b], P. Arminjon [a,b,*]

[a] *Centre de Recherches Mathématiques, Université de Montréal, Montréal, Que., Canada H3C 3J7*
[b] *Département de Mathématiques et de Statistique, Université de Montréal, CP 6128 succ Centre-Ville, Montréal, Que., Canada H3C 3J7*

Received 28 February 2005; received in revised form 29 June 2005; accepted 15 July 2005
Available online 15 September 2005

Abstract

We present three-dimensional central finite volume methods for solving systems of hyperbolic equations. Based on the Lax–Friedrichs and Nessyahu–Tadmor one-dimensional central finite difference schemes, the numerical methods we propose involve an original and a staggered grid in order to avoid the resolution of the Riemann problems at the cell interfaces. The cells of the original grid are Cartesian (cubes with faces parallel to the axes) while those of the staggered grid are either Cartesian or diamond-shaped. We apply these methods and solve some ideal magnetohydrodynamics problems. To satisfy the solenoidal property of the magnetic field in the numerical solution, we present an adaptation of Evans and Hawley's constrained transport method for central schemes which we call "CTCS". The CTCS method is easy to implement, it deals directly with the computed solution and does not require any additional staggering for the magnetic field components; furthermore, it preserves the second-order accuracy of the base scheme. Even without the application of the CTCS procedure, our numerical base schemes do not break down, and may even in some cases deliver reasonable results. The diamond dual cell scheme has a slight advantage for shocks and contact discontinuities. Our numerical results are in good agreement with corresponding results appearing in the recent literature.

Keywords: Three-dimensional central schemes; Ideal magnetohydrodynamics; Constrained transport

1. Introduction

Following the introduction of one-dimensional central schemes by Nessyahu and Tadmor [15], several extensions to two and three space dimensions on Cartesian [2,14] or unstructured [1,3,4] grids have been

* Corresponding author. Tel.: +1 514 484 6164; fax: +1 514 343 5700.
E-mail addresses: touma@dms.umontreal.ca (R. Touma), arminjon@crm.umontreal.ca (P. Arminjon).

0021-9991/$ - see front matter
doi:10.1016/j.jcp.2005.07.013

proposed for solving systems of hyperbolic equations. In this paper we propose two second-order accurate central schemes to solve three-dimensional systems of hyperbolic conservation laws and in particular problems in ideal magnetohydrodynamics.

When solving ideal MHD problems, the accumulation of numerical errors such as the truncation or round-off errors can usually lead to a non-physical phenomenon known as magnetic monopoles (when $\nabla \cdot \mathbf{B} \neq 0$). As a consequence, negative pressures and densities and other non-physical waves can arise as described in [8]. Based on experimental observations, the expression of **B** given by Biot and Savart's law leads to the existence of a magnetic vector potential **A**, and therefore to Maxwell's equation $\nabla \cdot \mathbf{B} = 0$, which should be satisfied for all practical purposes. Several approaches have been proposed to satisfy this constraint. Brackbill and Barnes [8] proposed their "projection scheme", involving the resolution of a Poisson equation, while Powell proposed his so-called "eight wave formulation" [17–19].

Another interesting approach is Evans and Hawley's [12] constrained transport method (CT), originally presented for finite difference schemes, where the induction equation is discretized using a staggered magnetic field. Several extensions of this method were later presented by Dai and Woodward [10], Balsara and Spicer [7], Ryu et al. [21], and Tóth [24], who has shown that the staggered magnetic field can be avoided. Now for central schemes, which rest on the use of an original and a dual staggered grid, none of the existing CT methods could be directly adopted.

In [5], we have adapted two-dimensional central schemes to MHD problems by introducing a new constrained transport-type divergence treatment ("CTCS"). The base scheme used a Cartesian original grid, and a staggered dual grid with diamond-shaped cells. The CTCS method we constructed preserves second-order accuracy and does not require any staggering of the magnetic field. The numerical experiments we presented in [5] are in good agreement with those appearing in the literature.

Recently Balbas et al. [6] have used 2D central schemes with Cartesian original and dual cells to solve ideal MHD problems; to enforce the divergence constraint, they used Brackbill and Barnes' projection method.

In this paper, we present two three-dimensional central schemes to solve ideal MHD problems. The numerical base scheme uses an original Cartesian grid and a staggered grid with either Cartesian or diamond-shaped dual cells. We construct a new adaptation (CTCS) of the constrained transport method to treat the non-vanishing magnetic field divergence. This approach preserves the second-order accuracy of the base scheme. Furthermore, it does not require any staggering of the magnetic field components.

Recently, Ziegler [27] presented an MHD solver which involves a semi-discrete central scheme for solving the hyperbolic system consisting of the conservation, momentum and energy equations, while Faraday's law is integrated separately using an adapted version of the CT scheme, with staggered magnetic field components. By contrast, the numerical base scheme proposed here is used to solve the complete set of the (eight) ideal MHD equations and we then apply the CTCS method to treat the magnetic field; the magnetic field in the numerical solution obtained using the base scheme is used to compute the electric field at time $t^{n+1/2}$ to ensure second order accuracy.

The numerical results we show in this paper compare very well with those appearing in the recent literature; the numerical magnetic field divergence we observe for the problems considered here remains of the order of 10^{-12}.

2. Equations of ideal magnetohydrodynamics

We consider in this paper the Ideal MHD equations written in their conservation form as:

$$\frac{\partial}{\partial t}\begin{bmatrix}\rho\\ \rho\mathbf{v}\\ \rho e\\ \mathbf{B}\end{bmatrix}+\nabla\cdot\begin{bmatrix}\rho\mathbf{v}\\ \rho\mathbf{v}\mathbf{v}+I(p+\frac{\mathbf{B}\cdot\mathbf{B}}{2})-\mathbf{B}\mathbf{B}\\ (\rho e+p+\frac{\mathbf{B}\cdot\mathbf{B}}{2})\mathbf{v}-(\mathbf{v}\cdot\mathbf{B})\mathbf{B}\\ \mathbf{v}\mathbf{B}-\mathbf{B}\mathbf{v}\end{bmatrix}=0. \tag{1}$$

The system (1) describes the conservation of the mass density ρ, momentum $\rho\mathbf{v}$, and total energy ρe. Faraday's law describes the evolution of the magnetic field $\mathbf{B}$. The thermal pressure is computed from an ideal gas equation of state,

$$p=(\gamma-1)\left(\rho e-\frac{1}{2}\rho|\mathbf{v}|^2-\frac{1}{2}|\mathbf{B}|^2\right), \tag{2}$$

where γ denotes the ratio of specific heats.

3. Multidimensional central schemes

In this section, we present the three-dimensional central schemes we are going to use as base schemes for solving ideal MHD problems. The original cells are Cartesian (uniform cubes), the staggered dual cells can be either Cartesian or diamond-shaped cells.

3.1. Three-dimensional central scheme with Cartesian dual staggered cells

We consider the following initial value problem:

$$\begin{cases}\vec{U}_t+\nabla\cdot\mathbf{F}=\vec{U}_t+\vec{f}_x+\vec{g}_y+\vec{h}_z=0,\ t>0,\\ \vec{U}(x,y,z,t=0)=\vec{U}_0(x,y,z).\end{cases} \tag{3}$$

The system (3) is assumed to be hyperbolic (the subscripts denote partial differentiation with respect to corresponding variables). We consider for our computational domain a uniform parallelepiped-shaped grid. Starting from the original Cartesian grid with cells $C_{i,j,k}\equiv[x_{i-1/2},x_{i+1/2}]\times[y_{j-1/2},y_{j+1/2}]\times[z_{k-1/2},z_{k+1/2}]$ (solid-line cubes centered at nodes (x_i,y_j,z_k)), at time t^n, we alternate to the dual staggered cell $D_{i+1/2,j+1/2,k+1/2}\equiv[x_i,x_{i+1}]\times[y_j,\ y_{j+1}]\times[z_k,z_{k+1}]$ (dashed-line cubes centered at nodes $(x_{i+1/2},y_{j+1/2},z_{k+1/2})$) at time t^{n+1}, and return back to the original cell $C_{i,j,k}$ at time t^{n+2} as shown in Fig. 1. We suppose that the solution is given at time t^n on the original cells; in a first time step, we want to compute the solution of system (3) on the staggered dual cells using as initial conditions the solution at time t^n. We shall denote

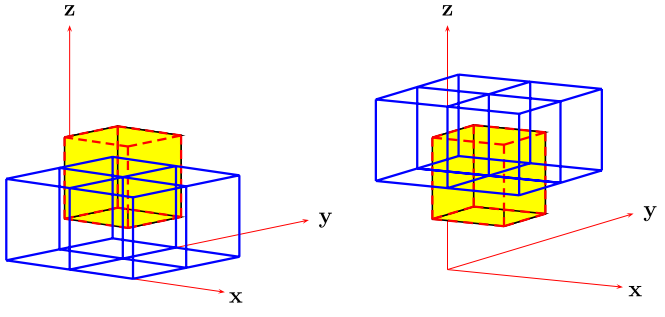

Fig. 1. One dual cell (dashed line cube) intersects two layers of four original cells (solid line cubes).

the dual cell $D_{i+1/2,j+1/2,k+1/2}$ by the shorter notation $\mathscr{D}_{i,j,k}$. Integrating the conservation law (3) on the domain $\Omega = \mathscr{D}_{i,j,k} \times [t^n, t^{n+1}]$, we obtain

$$\int_{\mathscr{D}_{i,j,k}} \vec{U}(x,y,z,t^{n+1})\,\mathrm{d}V = \int_{\mathscr{D}_{i,j,k}} \vec{U}(x,y,z,t^n)\,\mathrm{d}V - \int_{t_n}^{t_n+1} \int_{\mathscr{D}_{i,j,k}} \nabla\cdot\vec{F}(\vec{U}(x,y,z,t))\,\mathrm{d}V\,\mathrm{d}t. \tag{4}$$

The left-hand side of Eq. (4) defines the value of the solution at time t^{n+1} on the staggered dual cell $\mathscr{D}_{i,j,k}$. Let $\{C_{ds}\}_{s=1,\ldots,4}$ denote the four uniform cubes centered at the points (x_i,y_j,z_k), (x_{i+1},y_j,z_k), (x_{i+1},y_{j+1},z_k), (x_i,y_{j+1},z_k), and $\{C_{us}\}_{s=1,\ldots,4}$ denote the cubes centered at (x_i,y_j,z_{k+1}), (x_{i+1},y_j,z_{k+1}), $(x_{i+1},y_{j+1},z_{k+1})$, and (x_i,y_{j+1},z_{k+1}). The integral of $\vec{U}(x,y,z,t^n)$ on the dual cell $\mathscr{D}_{i,j,k}$ in Eq. (4) is split into eight integrals as follows:

$$\int_{\mathscr{D}_{i,j,k}} \vec{U}(x,y,z,t^n)\,\mathrm{d}V = \sum_{r\in\{u,d\}} \sum_{s=1}^{s=4} \int_{\mathscr{D}_{i,j,k}\cap C_{rs}} \vec{U}(x,y,z,t^n)\,\mathrm{d}V. \tag{5}$$

Applying van Leer's "MUSCL" piecewise linear interpolants [26] defined at the center of cell $C_{i,j,k}$ by:

$$\vec{U}_{ijk}(x,y,z,t^n) \simeq \vec{U}^n_{ijk} + \frac{x-x_i}{\Delta x}\vec{U}^{\lim}_{i,j,k;x} + \frac{y-y_j}{\Delta y}\vec{U}^{\lim}_{i,j,k;y} + \frac{z-z_k}{\Delta z}\vec{U}^{\lim}_{i,j,k;z}, \tag{6}$$

will guarantee second-order accuracy and preserve the monotonicity. Here $(\nabla\vec{U})^{\lim} \equiv (\vec{U}^{\lim}_x/\Delta x, \vec{U}^{\lim}_y/\Delta y, \vec{U}^{\lim}_z/\Delta z)$ is a limited numerical gradient; hence for $r=d$, $s=1$ we obtain

$$\begin{aligned}\int_{\mathscr{D}_{i,j,k}\cap C_{d1}} \vec{U}(x,y,z,t^n)\,\mathrm{d}V &\simeq \vec{U}(x_i+h/4, y_j+h/4, z_k+h/4, t^n)\mathscr{V}(\mathscr{D}_{i,j,k}\cap C_{d1}) \\ &\simeq \left\{\vec{U}_{i,j,k} + \frac{1}{4}\vec{U}^{\lim}_{i,j,k;x} + \frac{1}{4}\vec{U}^{\lim}_{i,j,k;y} + \frac{1}{4}\vec{U}^{\lim}_{i,j,k;z}\right\}\frac{h^3}{8},\end{aligned} \tag{7}$$

where $h=\Delta x=\Delta y=\Delta z$ and $\mathscr{V}(\mathscr{D}_{i,j,k}\cap C_{r,s}) = h^3/8, r\in\{u,d\}, s=1,\ldots,4$ denotes the volume of one of the eight partial cubes that form the dual cell. In a similar manner we compute each integral in the summation in Eq. (5).

For the second integral in the right-hand side (RHS) of Eq. (4), the divergence theorem gives

$$\int_{t_n}^{t_n+1} \int_{\mathscr{D}_{i,j,k}} \nabla\cdot\vec{F}(\vec{U}(x,y,z,t))\,\mathrm{d}V\,\mathrm{d}t = \int_{t_n}^{t_n+1} \int_{\partial\mathscr{D}_{i,j,k}} \vec{F}(\vec{U}(x,y,z,t))\cdot\vec{n}\,\mathrm{d}A\,\mathrm{d}t. \tag{8}$$

Here $\vec{n}$ denotes the unit normal vector to $\partial\mathscr{D}_{i,j,k}$. The flux integral with respect to time in Eq. (8) is approximated to second-order accuracy using the midpoint rule. For the predicted values of the flux at the intermediate time we use a first-order accurate Taylor expansion and the conservation law:

$$\vec{U}^{n+1/2} \simeq \vec{U}^n + \frac{\Delta t}{2}\vec{U}^n_t = \vec{U}^n - \frac{\Delta t}{2}\nabla\cdot\vec{F}^n; \vec{F}^{n+1/2} = \vec{F}(\vec{U}^{n+1/2}). \tag{9}$$

Eq. (9) can be written using the Jacobian matrices (A,B,C) of the flux functions $(\vec{f},\vec{g},\vec{h})$ as follows:

$$\vec{U}^{n+1/2} \simeq \vec{U}^n - \frac{\Delta t}{2h}(A(\vec{U}^n)\vec{U}^{\lim}_x + B(\vec{U}^n)\vec{U}^{\lim}_y + C(\vec{U}^n)\vec{U}^{\lim}_z). \tag{10}$$

Alternately, one could instead directly apply a flux limiting procedure in Eq. (9) without using the jacobian matrices, which may accelerate the computations (jacobian-free form (JFF) [6]).

We then write the flux integral in the RHS of Eq. (8) as a sum of integrals over the six faces $(S_r, r=1,\ldots,6)$ of the dual cell and write for instance the integral over S_1 (with normal $\vec{n}_1=(1,0,0)$) to second-order accuracy as follows:

$$\int_{S_1} \vec{F}(\vec{U}(x,y,z,t^{n+1/2}))\cdot\vec{n}_1\,\mathrm{d}A \simeq \frac{h^2}{4}(\vec{f}^{\,n+1/2}_{i+1,j,k}+\vec{f}^{\,n+1/2}_{i+1,j+1,k}+\vec{f}^{\,n+1/2}_{i+1,j,k+1}+\vec{f}^{\,n+1/2}_{i+1,j+1,k+1}), \tag{11}$$

with similar formulas for the fluxes across the faces $S_2,\ldots,S_6$, which allows us to compute $\vec{U}^{n+1}_{i+1/2,j+1/2,k+1/2}$. Applying a similar algorithm leads to the values $\vec{U}^{n+2}_{i,j,k}$ on the original grid.

3.2. Three-dimensional central scheme with diamond staggered dual cells

Another choice for the dual cells of the staggered grid is the three-dimensional extension of the diamond staggered cell scheme we previously considered in [5]. For our computational domain, we consider a parallelepiped-shaped domain uniformly discretized with Cartesian cubic cells $C_{i,j,k}\equiv[x_{i-1/2},x_{i+1/2}]\times[y_{i-1/2},y_{i+1/2}]\times[z_{i-1/2},z_{i+1/2}]$, centered at the nodes $a_{i,j,k}$. For the staggered dual cells, we consider the diamond shaped cells obtained by joining the centers of two adjacent Cartesian cells $C_{i,j,k}$ and $C_{i+1,j,k}$ to their common interface as in Fig. 2; the resulting cell is denoted by $D_{i+1/2,j,k}$. We suppose that the solution $\vec{U}^n_{i,j,k}$ is given at time $t=t^n$ on the original Cartesian cells $C_{i,j,k}$. We consider the cells $C_{i,j,k}$ and $C_{i+1,j,k}$ centered at the nodes $c_l=(x_i,y_j,z_k)$ and $c_r=(x_{i+1},y_j,z_k)$, respectively, and such that the line $c_l\,c_r$ is parallel to the x-axis as in Fig. 3. We integrate Eq. (3) on the domain $D_{i+1/2,j,k}\times[t^n,t^{n+1}]$ and apply the divergence theorem, obtaining

$$\int_{D_{i+1/2,j,k}} \vec{U}(x,y,z,t^{n+1})\,\mathrm{d}V = \int_{D_{i+1/2,j,k}} \vec{U}(x,y,z,t^{n})\,\mathrm{d}V - \int_{t_n}^{t_n+1}\int_{\partial D_{i+1/2,j,k}} \vec{F}(\vec{U}(x,y,z,t^n))\cdot\vec{n}\,\mathrm{d}A\,\mathrm{d}t. \tag{12}$$

The left-hand side of Eq. (12) defines the average value of the solution $\vec{U}^{n+1}_{i+1/2,j,k}$ on the staggered dual cell; $\vec{n}$ denotes the unit outward normal vector to the boundary $\partial D_{i+1/2,j,k}$ of the dual cell. With the help of van Leer's MUSCL-type linear interpolants [26], we approximate to second-order accuracy the first integral of the RHS of Eq. (12) as follows:

$$\int_{D_{i+1/2,j,k}} \vec{U}(x,y,z,t^n)\,\mathrm{d}V \simeq \frac{h^3}{6}\left[\vec{U}^n_{i,j,k}+\vec{U}^n_{i+1,j,k}+\frac{2}{5}(\vec{U}^{\lim}_{i,j,k;x}-\vec{U}^{\lim}_{i+1,j,k;x})\right]. \tag{13}$$

For the second integral in the RHS of Eq. (12), we use the midpoint formula for the time integration

$$\int_{t_n}^{t_n+1}\int_{\partial D_{i+1/2,j,k}} \vec{F}(\vec{U}(x,y,z,t^n))\cdot\vec{n}\,\mathrm{d}A\,\mathrm{d}t \simeq \Delta t\int_{\partial D_{i+1/2,j,k}} \vec{F}(\vec{U}(x,y,z,t^{n+1/2}))\cdot\vec{n}\,\mathrm{d}A. \tag{14}$$

Before computing the flux integral across the area $\partial D_{i+1/2,j,k}$ we need to introduce the following notations:

(1) For the Cartesian cells $C_{i,j,k}$ and $C_{i+1,j,k}$:

- $c_l=(x_i,y_j,z_k)$ and $c_r=(x_{i+1},y_j,z_k)$ denote the centers of the adjacent cells $C_{i,j,k}$ and $C_{i+1,j,k}$.

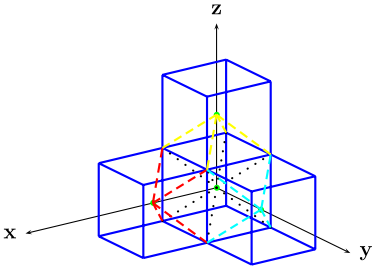

Fig. 2. Original Cartesian cells (solid-line cubes) and dual diamond cells (dashed-lines).

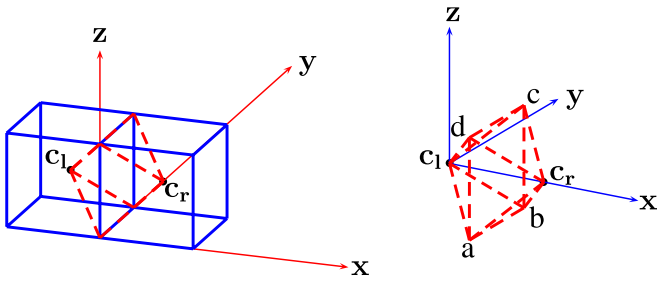

Fig. 3. Two Cartesian cells $C_{i,j,k}$, $C_{i+1,j,k}$ (solid line cubes) and dual diamond cell $D_{i+1/2,j,k}$ (dashed line).

- The nodes of the common interface of cells $C_{i,j,k}$ and $C_{i+1,j,k}$ are:
- a: $(x_i+h/2, y_j-h/2, z_k-h/2)$, c: $(x_i+h/2, y_j+h/2, z_k+h/2)$,
- b: $(x_i+h/2, y_j+h/2, z_k-h/2)$, d: $(x_i+h/2, y_j-h/2, z_k+h/2)$.

(2) For the diamond dual cell ($D_{i+1/2,j,k}$):

$T_l^k|_{k=1,\ldots,4}$ denotes the triangles $c_{l\,\mathrm{cd}}$, $c_{l\,\mathrm{ad}}$, $c_{l\,\mathrm{cb}}$, $c_{l\,\mathrm{ab}}$ with center at e_l^k, respectively, with unit outward normal $\vec{n}_l^k$.
$T_r^k|_{k=1,\ldots,4}$ denotes the triangles $c_{r\,\mathrm{cd}}$, $c_{r\,\mathrm{ad}}$, $c_{r\,\mathrm{cb}}$, $c_{r\,\mathrm{ab}}$ with center at e_r^k, respectively, with unit outward normal $\vec{n}_r^k$.

To approximate the flux-integral across $\partial D_{i+1/2,j,k}$ with second-order quadrature, we obtain predictions of both $\vec{U}^{n+1/2}_{\partial D_{i+1/2,j,k}}$ and $\vec{F}^{n+1/2}_{\partial D_{i+1/2,j,k}}$ at time $t^{n+1/2}$ using Taylor expansions with respect to t; we evaluate the approximations at the centers e_l^k and e_r^k of the triangles T_l^k and T_r^k ($k=1,\ldots,4$) as follows:

$$\vec{U}^{n+1/2}_{T_s^k} \simeq \vec{U}_s(e_s^k, t^n) + \frac{\Delta t}{2}\vec{U}_t(e_s^k, t^n),\ s = l, r \text{ and } k = 1,\ldots,4. \tag{15}$$

Eq. (15) is approximated as previously using van Leer's linear interpolants as well as the conservation law (3). The flux-integral can finally be computed as follows:

$$\begin{aligned}
&\int_{\partial D_{i+1/2,j,k}} \vec{F}(\vec{U}(x,y,z,t^{n+1/2}))\cdot\vec{n}\,\mathrm{d}A \\
&\simeq \frac{\mathscr{A}(T)}{\sqrt{2}}\cdot\Big[\Big\{-\vec{f}(\vec{U}^{n+1/2}_{e_l^1}) + \vec{h}(\vec{U}^{n+1/2}_{e_l^1})\Big\} + \Big\{\vec{f}(\vec{U}^{n+1/2}_{e_r^1}) + \vec{h}(\vec{U}^{n+1/2}_{e_r^1})\Big\} + \Big\{-\vec{f}(\vec{U}^{n+1/2}_{e_l^2}) - \vec{g}(\vec{U}^{n+1/2}_{e_l^2})\Big\} \\
&\quad + \Big\{\vec{f}(\vec{U}^{n+1/2}_{e_r^2}) - \vec{g}(\vec{U}^{n+1/2}_{e_r^2})\Big\} + \Big\{-\vec{f}(\vec{U}^{n+1/2}_{e_l^3}) + \vec{g}(\vec{U}^{n+1/2}_{e_l^3})\Big\} + \Big\{\vec{f}(\vec{U}^{n+1/2}_{e_r^3}) + \vec{g}(\vec{U}^{n+1/2}_{e_r^3})\Big\} \\
&\quad + \Big\{-\vec{f}(\vec{U}^{n+1/2}_{e_l^4}) - \vec{h}(\vec{U}^{n+1/2}_{e_l^4})\Big\} + \Big\{\vec{f}(\vec{U}^{n+1/2}_{e_r^4}) - \vec{h}(\vec{U}^{n+1/2}_{e_r^4})\Big\}\Big] = \frac{\mathscr{A}(T)}{\sqrt{2}}\mathrm{RHS},
\end{aligned} \tag{16}$$

where $\mathscr{A}(T) = \frac{h^2}{2\sqrt{2}}$ denotes the area of the triangle $T(\mathscr{A}(T_l^k) = \mathscr{A}(T_r^k) = \mathscr{A}(T))$. The solution at time t^{n+1} on the dual cell $D_{i+1/2,j,k}$ takes the form:

$$\vec{U}^{n+1}_{i+1/2,j,k} = \frac{1}{2}(\vec{U}^n_{i,j,k} + \vec{U}^n_{i+1,j,k}) + \frac{1}{5}(\vec{U}^{\lim}_{i,j,k;x} - \vec{U}^{\lim}_{i+1,j,k;x}) - \frac{3\Delta t}{4h}\mathrm{RHS}. \tag{17}$$

In a similar manner we compute the solution at time t^{n+1} on the dual cells $D_{i,j+1/2,k}$ and $D_{i,j,k+1/2}$. The solution on the original Cartesian cells will be recovered at time t^{n+2} using an appropriately modified procedure.

4. Divergence-free magnetic field requirement and some numerical approaches

If, in the solution of a specific ideal MHD problem, the initial magnetic field $\mathbf{B}$ satisfies the $\nabla \cdot \mathbf{B} = 0$ constraint, it is easily proved that it will satisfy it at all time. Unfortunately, the numerical solution rarely displays this property: due to truncation and round-off errors, the divergence builds up to non-negligible values, which can lead to the breakdown of the numerical solution. Among several methods proposed to induce the magnetic field to satisfy the divergence constraint, we consider here Evans and Hawley's constrained transport (CT) approach [12] as it was already successfully tested in quite a few papers.

The original version of the CT method uses the magnetic field $\mathbf{B}$ at the cell centers, and computes by linear interpolation a staggered magnetic field $\mathbf{b}$ at the cell interface midpoints; the components of the staggered magnetic field $\mathbf{b}$ are then treated, using a special symmetric discretization of the induction equation, so as to satisfy the divergence constraint. More recently, Tóth [24] has observed that this staggering is not essential, and he reformulated each of the existing staggered versions of the CT method (Evans and Hawley [12], Dai and Woodward [10], Balsara and Spicer [7], Ryu et al. [21]) into unstaggered methods.

As we have seen in the previous section, the numerical schemes we use require an original and a staggered grid and thus, none of the existing versions of the CT method could be applied directly. Here we propose two three-dimensional CTCS adaptations of the CT method that apply to three-dimensional central schemes with Cartesian or diamond-shaped dual cells, respectively. This CTCS approach directly deals with the cell-centered magnetic field components and does not require any additional staggering.

Here we present the CTCS method for three-dimensional central schemes with diamond-shaped dual cells. Let $U^n_{i,j,k}$ denote the solution at time t^n on the Cartesian cell $C_{i,j,k}$, and let $U^{n+1}_{i+1/2,j,k}$ denote the solution at time t^{n+1} on the staggered dual cell $D_{i+1/2,j,k}$. We suppose that the constraint $\nabla \cdot \mathbf{B}^n_{i,j,k} = 0$ is satisfied i.e., the central difference discretization of the divergence operator of the magnetic field satisfies

$$\nabla \cdot \mathbf{B}^n_{i,j,k} \simeq \frac{B^{n,x}_{i+1,j,k} - B^{n,x}_{i-1,j,k}}{2\Delta x} + \frac{B^{n,y}_{i,j+1,k} - B^{n,y}_{i,j-1,k}}{2\Delta y} + \frac{B^{n,z}_{i,j,k+1} - B^{n,z}_{i,j,k-1}}{2\Delta z} = 0. \tag{18}$$

We want to compute the divergence-free magnetic field components of $\mathscr{B}^{n+1}_{i+1/2,j,k}$ on the dual cells, using the base scheme-updated magnetic field $\mathscr{B}^{*}_{i+1/2,j,k}$ at time $t = t^{n+1}$, without any additional staggering of $\mathscr{B}$. Fig. 4 shows the required cells to compute $\nabla \cdot \mathscr{B}^{n+1}_{i+1/2,j,k}$.

We first compute the electric field $\mathbf{E}^{n+1/2}_{i+1/2,j,k} = (\Omega^x, \Omega^y, \Omega^z)^{n+1/2}_{i+1/2,j,k}$ at time $t^{n+1/2}$ using the data at time t^n and t^{n+1}, on the original and the dual staggered grids, respectively, as follows:

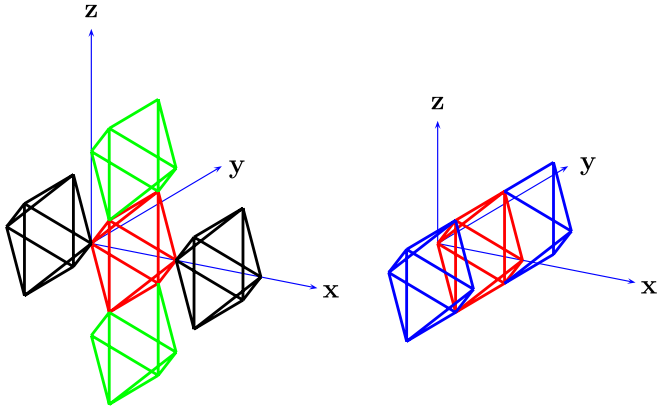

Fig. 4. Six dual cells along the x and z directions (left) and the y direction (right) are required to compute $\nabla \cdot \mathscr{B}^{n+1}_{i+1/2,j,k}$.

$$\mathbf{E}^{n+1/2}_{i+1/2,j,k} = -(\mathbf{v}\times\mathbf{B})^{n+1/2}_{i+1/2,j,k} = -\frac{1}{2}\left[(\mathbf{v}^{n+1}\times\mathscr{B}^{*})_{i+1/2,j,k} + \frac{1}{2}\{(\mathbf{v}\times\mathbf{B})^{n}_{i,j,k} + (\mathbf{v}\times\mathbf{B})^{n}_{i+1,j,k}\}\right]. \tag{19}$$

This discretization will ensure second-order accuracy with respect to time. Next, we discretize the induction equation

$$\partial_t\mathbf{B} + \nabla\times\mathbf{E} = 0, \tag{20}$$

on the $D_{i+1/2,j,k}-$type staggered dual cells using the following centered differences:

$$\mathscr{B}^{n+1,x}_{i+1/2,j,k} = \frac{1}{2}(B^{n,x}_{i,j,k} + B^{n,x}_{i+1,j,k}) - \Delta t\frac{\Omega^{n+1/2,z}_{i+1/2,j+1,k} - \Omega^{n+1/2,z}_{i+1/2,j-1,k}}{2\Delta y} + \Delta t\frac{\Omega^{n+1/2,y}_{i+1/2,j,k+1} - \Omega^{n+1/2,y}_{i+1/2,j,k-1}}{2\Delta z}, \tag{21}$$

$$B^{n+1,y}_{i+1/2,j,k} = \frac{1}{2}(B^{n,y}_{i,j,k} + B^{n,y}_{i+1,j,k}) - \Delta t\frac{\Omega^{n+1/2,x}_{i+1/2,j,k+1} - \Omega^{n+1/2,x}_{i+1/2,j,k-1}}{2\Delta z} + \Delta t\frac{\Omega^{n+1/2,z}_{i+3/2,j,k} - \Omega^{n+1/2,z}_{i-1/2,j,k}}{2\Delta x}, \tag{22}$$

$$B^{n+1,z}_{i+1/2,j,k} = \frac{1}{2}(B^{n,z}_{i,j,k} + B^{n,z}_{i+1,j,k}) - \Delta t\frac{\Omega^{n+1/2,y}_{i+3/2,j,k} - \Omega^{n+1/2,y}_{i-1/2,j,k}}{2\Delta x} + \Delta t\frac{\Omega^{n+1/2,x}_{i+1/2,j+1,k} - \Omega^{n+1/2,x}_{i+1/2,j-1,k}}{2\Delta y}. \tag{23}$$

This special discretization of the induction equation and the particular choice of the electric field at the intermediate time $t^{n+1/2}$ will conserve the second order accuracy of the base scheme. A tedious but straightforward calculation allows us to prove that:

$$\nabla\cdot\mathscr{B}^{n+1}_{i+1/2,j,k} = \frac{1}{2}\{\nabla\cdot\mathbf{B}^{n}_{i,j,k} + \nabla\cdot\mathbf{B}^{n}_{i+1,j,k}\}. \tag{24}$$

Hence, if the magnetic field at time t^n is solenoidal, the CTCS-updated magnetic field will conserve the same property, and thus $\nabla\cdot\mathscr{B}^{n+1}_{i+1/2,j,k} = 0$. The magnetic field on the cells $\{D_{i,j+1/2,k}\}$ and $\{D_{i,j,k+1/2}\}$ can be handled in a similar way. The CTCS divergence treatment in the purely Cartesian case can be found in Appendix A.

5. Numerical experiments

The fact that central schemes require an original and a staggered grid to avoid solving the Riemann problems [13] at the cell interfaces represents a restriction on the computation of the time step as compared to other numerical methods. As described in [15] for the 1D case, and later in [1,14] for the multidimensional central schemes, the CFL number for central schemes is about 0.5. Even with this time-step restriction, experience has shown that the computing times of central schemes are substantially shorter than those of methods based on exact or approximate Riemann solvers. The numerical results we present later in this section are obtained using a CFL number of 0.475. It is also known that, in the case of central schemes as well as other numerical methods, the choice of the limiter in the numerical computation of gradients may contribute in a significant way to the quality of the numerical resolution.

Before considering MHD problems, we first verify and compare our numerical base schemes (diamond and Cartesian dual cell schemes) by considering a simple three-dimensional scalar advection problem with continuous or non-continuous initial data. We consider the following three-dimensional scalar advection equation:

$$\begin{cases} u_t + u_x + u_y + u_z = 0, \\ u(x,y,z)|_{t=0} = u_0(x,y,z). \end{cases} \tag{25}$$

The analytic exact solution of Eq. (25) at a time t, and at a point (x, y, z) is obtained from the initial data as $u(x, y, z, t) = u_0(x - t, y - t, z - t)$. We consider for our computational domain the cube $[0, 1]^3$ uniformly discretized with 100^3 gridpoints. We consider non-continuous initial data given as follows:

$$u_0(x, y, z) = \begin{cases} 4 & \text{if } (x - 0.5)^2 + (y - 0.5)^2 + (z - 0.5)^2 \leqslant 0.15^2, \\ 1 & \text{elsewhere.} \end{cases} \tag{26}$$

Fig. 5 shows the numerical solution ("o") and the exact solution (solid line) at time $t = 0.0522$. We have computed the numerical order of both schemes using for non-continuous initial data the function defined in Eq. (26), and for continuous initial data, the following function:

$$u_0(x, y, z) = \sin(2\pi x) \sin(2\pi y) \sin(2\pi z). \tag{27}$$

As shown in Table 1, the second-order accuracy of the schemes is verified when continuous initial data are used. In the case of non-continuous initial data, it is well known that the numerical solution is going to be at most first-order accurate; this is also shown in Table 1 for both numerical base schemes.

5.1. Shock-tube problem

Another interesting experiment that one may consider is the three-dimensional adaptation of Sod's shock tube problem [23] for the Euler equations which can be obtained from the ideal MHD equations by simply dropping the magnetic field components in system (1). The initial data for this test feature a shock along the plane $x = 0.5$; the two constant states are $U_l = [1, 0, 0, 0, 1]$ (if $0 < x < 0.5$) and $U_r = [0.125, 0, 0, 0, 0.1]$ (if $0.5 < x < 1$) for $U = [\rho, \rho u_x, \rho u_y, \rho u_z, \rho e]$. The adiabatic constant is $\gamma = 1.4$. The numerical solution is computed at time $t = 0.164$ using the diamond dual cell scheme and the Cartesian dual cell scheme; the computational domain is uniformly discretized using 200 points along the x-axis and 40 points along each of the y and z axes. Fig. 6 shows a comparison between our numerical results (dotted lines) obtained with diamond dual cells (left) and Cartesian dual cells (right), and the exact solution (solid line) of the corresponding one-dimensional problem. For these calculations, we have used the MC-θ limiter with $\theta = 1.5$.

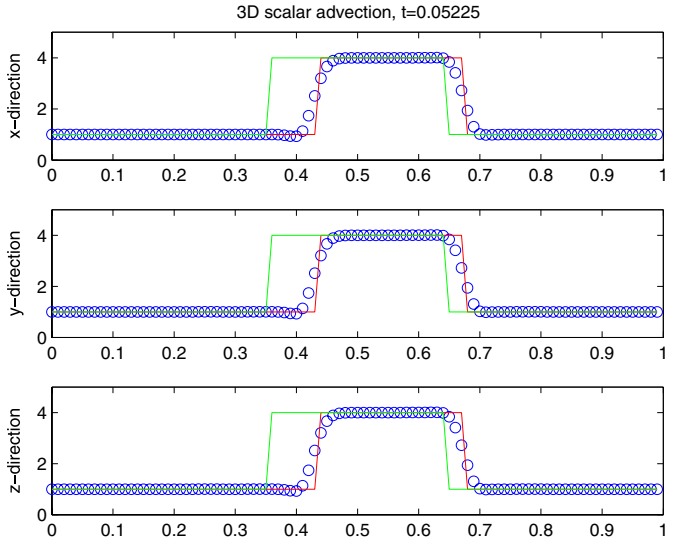

Fig. 5. Solution of the scalar advection equation, three snapshots along the axes of the system; the initial data is shown in solid line, the exact solution and the numerical solution are shown in solid line and in "o" respectively.

Table 1
Numerical order of the base schemes for smooth or non-continuous initial data

Method	Smooth initial data	Non-continuous initial data
Cartesian dual cells	1.901265	0.996402
Diamond dual cells	2.000029	0.998725

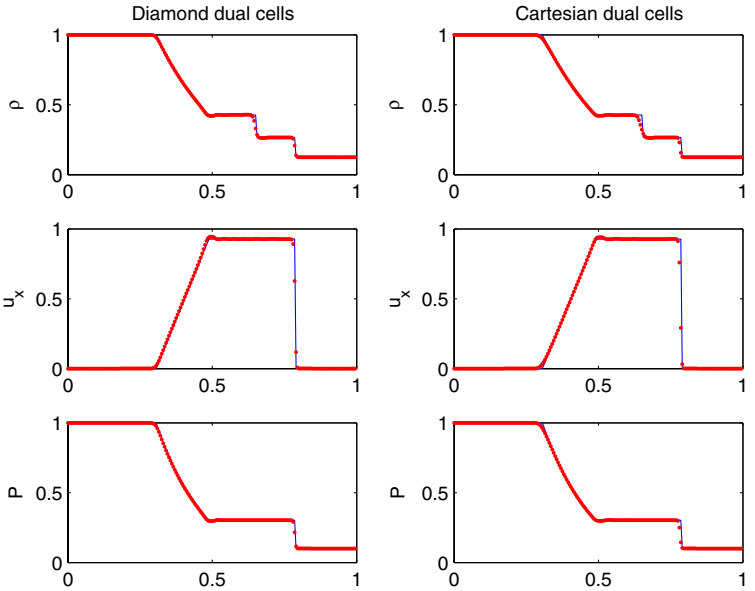

Fig. 6. Numerical solution of the three-dimensional Sod shock-tube problem obtained using diamond dual cell scheme (left) and Cartesian dual cell scheme (right).

The density profile is enlarged in Fig. 7 for a closer comparison of both methods. As can be seen when magnifying this figure, the diamond dual cell scheme leads to a slightly better resolution of the contact and shock waves. The relative error, computed as suggested in [24], for the numerical solution (vs. the exact solution) computed on 200 x-gridpoints using the Cartesian dual cell scheme is 0.0057213 while the error for diamond dual cell scheme is 0.0051303.

5.2. MHD shock-tube problem

We now consider a three-dimensional adaptation of the 1D MHD shock tube problem involving seven discontinuities; this test case was originally considered by Ryu and Jones [22]. The initial conditions feature a shock along the plane $x = 0$ with the following data: $U_r = [0.989112, -0.013123, 0.026933, 0.010037, 4.024421, 2.002600, 0.971588]$ (if $0 < x < 1$) and $U_l = [1.08, 1.2, 0.01, 0.5, 3.6, 2.0, 0.95]$ (if $-1 < x < 0$); here $U = [\rho, u_x, u_y, u_z, B_y, B_z, p]$, $B_x = 2$ and $\gamma = 5/3$. The computational domain is uniformly discretized with 200 grid points along the x-axis, 30 points along the y and z axes. We applied both numerical schemes involving Cartesian dual cells and diamond dual cells, and computed the solution at time $t = 0.4$. In both cases we compare (Figs. 8 and 9) the numerical results with the reference solution obtained, for the one-dimensional problem, using the numerical scheme proposed by Ryu and Jones [22] with 10000 gridpoints; this reference solution is also available online from the following address: http://www-ian.math.uni-magdeburg.de/anume/testcase/MHD/1d/rj/.

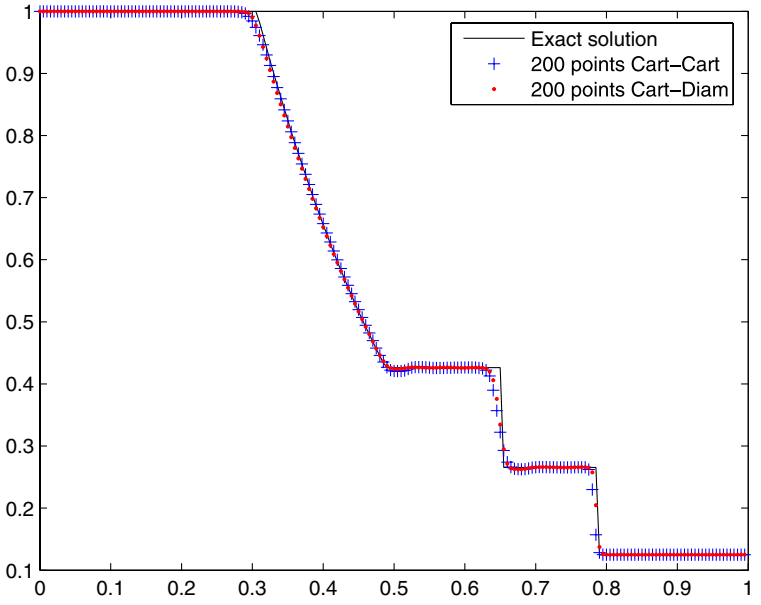

Fig. 7. Mass density along the x-axis for Sod's three-dimensional shock-tube problem.

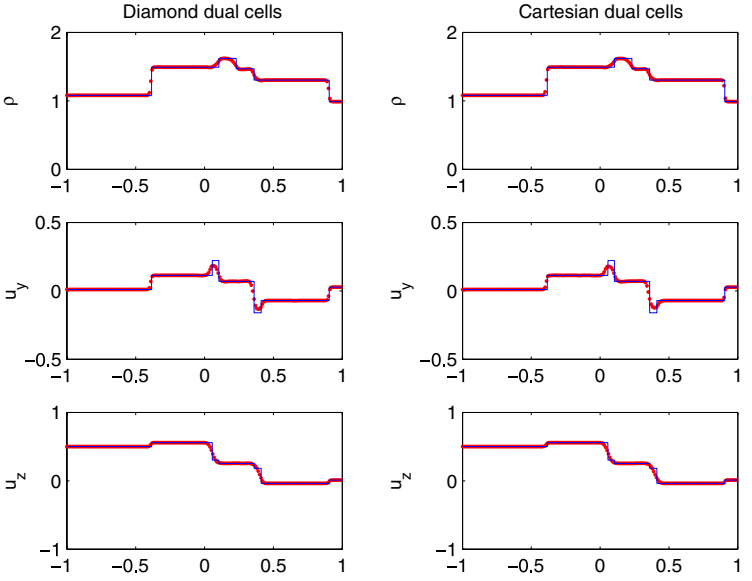

Fig. 8. Numerical solution of the three-dimensional MHD shock-tube problem obtained using the diamond dual cell scheme (left) and Cartesian dual cell scheme (right).

This is a very challenging test case due to the structure of its solution that involves seven constant states separated by shock waves and contact discontinuities. A good capture of the constant states requires a high definition discretization (we recall that the reference solution is obtained using 10000 grid points). On Figs.

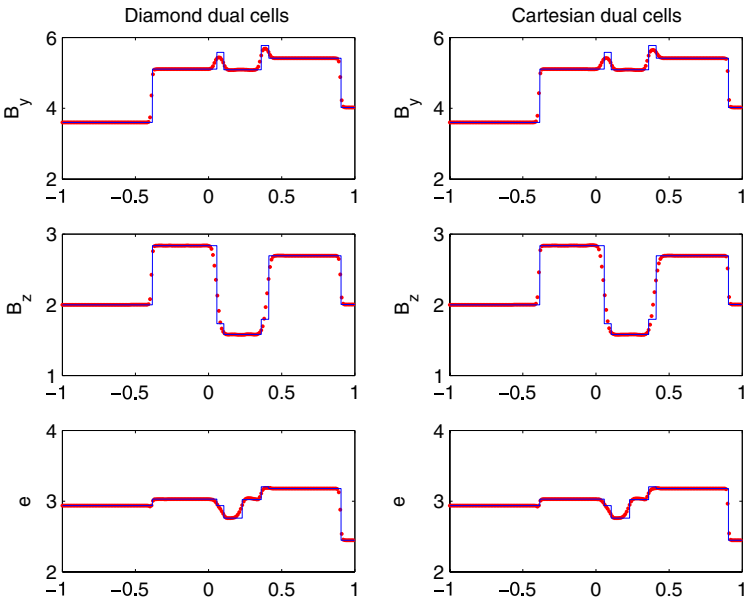

Fig. 9. Numerical solution of the three-dimensional MHD shock-tube problem obtained using the diamond dual cell scheme (left) and Cartesian dual cell scheme (right), continued.

8 and 9, computed with 200 gridpoints in the x-direction, the diamond-dual cell scheme seems to do slightly better than the Cartesian-dual cell scheme.

This is confirmed in Fig. 10, where we also included results obtained with 400 x-gridpoints and the diamond-dual cell scheme, which brings a substantial improvement on both 200 x-points results. The relative error for the numerical solution (vs. the reference solution) computed on 200 x-gridpoints using the Cartesian dual cell scheme is 0.00514746 while the error for diamond dual cell scheme is 0.00513999.

5.3. Orszag–Tang problems

Our next three-dimensional MHD problem is an Orszag–Tang-type problem [11,24,25]. The initial data for this problem are the following: $\rho(x,y,z)=\rho_0, p(x,y,z)=p_0, \mathbf{u}(x,y,z)=-\sin y\mathbf{i}+\sin x\mathbf{j}, \mathbf{B}(x,y,z)=-\sin y\mathbf{i}+\sin(2x)\mathbf{j}$, with $0\leqslant x,y\leqslant 2\pi, \rho_0=25/36$ and $p_0=5/3$. $\mathbf{i}$ and $\mathbf{j}$ are unit vectors in the x and y directions.

We have computed the numerical solution on a $100\times 100\times 100$ grid at time $t=0.5$ using both Cartesian and diamond dual cell schemes along with the corresponding CTCS approach to maintain a divergence-free magnetic field. Fig. 11(left) shows several slides in the three-dimensional space of the contour lines of the mass density; the arrows denote the magnitude of the velocity field. Fig. 11(right) shows the contours of the mass density in the plane $z=\pi$; this plot compares very well with the corresponding results for the two-dimensional problem we previously considered in [5] as well as those appearing in several recent papers in the literature [6,10,20,24]. Fig. 12(left) shows two plots of the mass density along the line $y=\pi$ of the plane $z=\pi$ obtained using both Cartesian (x-line) and diamond (dotted line) dual cell schemes at time $t=0.5$; the reference solution (solid line) is obtained using the two-dimensional diamond dual cell scheme on 400^2 gridpoints. Similarly, Fig. 12(right) shows the plot of the energy. Both methods yield almost undistinguishable results.

We now consider another Orszag–Tang-type problem, which is a slight modification of a problem considered in [16]; the initial data are as follows: $\rho(x,y,z)=\rho_0, p(x,y,z)=p_0,\ \mathbf{u}(x,y,z)=-\sin y\sin z\mathbf{i}+$

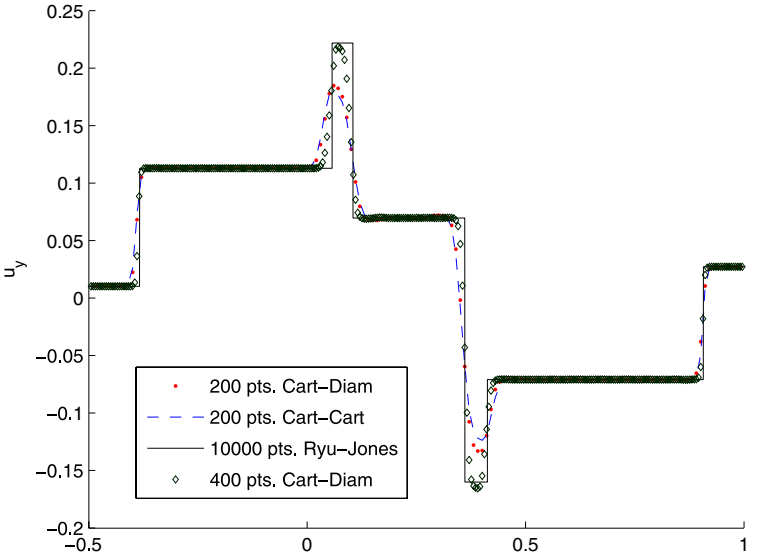

Fig. 10. Numerical solution of the three-dimensional MHD shock-tube problem obtained using the diamond dual cell scheme (dotted line) and Cartesian dual cell scheme (dashed line).

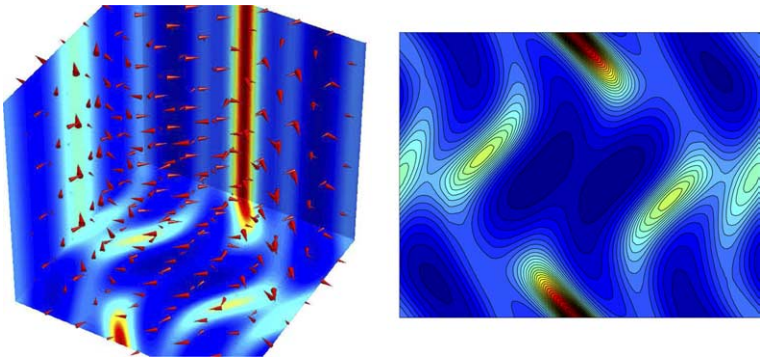

Fig. 11. Mass density (shaded contours) and velocity field magnitude (cone plot) for the Orszag–Tang problem at time $t = 0.5$ (left); contour lines of the mass density in the plane $z = \pi$ (right).

$\sin x \sin z\mathbf{j}$, $\mathbf{B}(x, y, z) = -\sin y \sin z\mathbf{i} + \sin(2x) \sin z\mathbf{j} + \sin(2x) \sin y\mathbf{k}$, with $0 \leqslant x, y, z \leqslant 2\pi, \rho_0 = 25/36$ and $p_0 = 5/3$. **i**, **j**, and **k** are the unit vectors in the x, y, and z directions, respectively. We have computed the solution at time $t = 0.5$ on 100^3 gridpoints using the Cartesian dual cell scheme; thanks to our CTCS divergence treatment, the maximum absolute value of the divergence observed for both Orszag–Tang vortex problems is of the order of 10^{-14}. Fig. 13(left) shows several isosurfaces of the mass density; Fig. 13(right) shows several slides, in three-dimensional-space, of the contour lines of the electric field magnitude. Fig. 14 shows the contours of the mass density and the energy in the plane $z = \pi$ at time $t = 0.5$. Fig. 15(left) shows the mass density contours in the plane $x = \pi/2$.

If we do not apply the CTCS divergence treatment, the base scheme can still reach the final time without showing instabilities: In fact, we have solved this Orszag–Tang problem using the diamond dual cell scheme on 50^3 gridpoints, without applying the CTCS divergence treatment. Fig. 15(right) shows the plots along

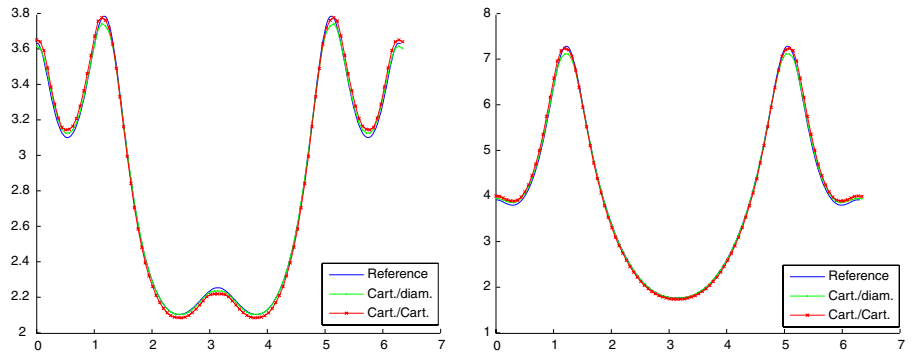

Fig. 12. Plot of the mass density (left) and the energy for the Orszag–Tang vortex problem.

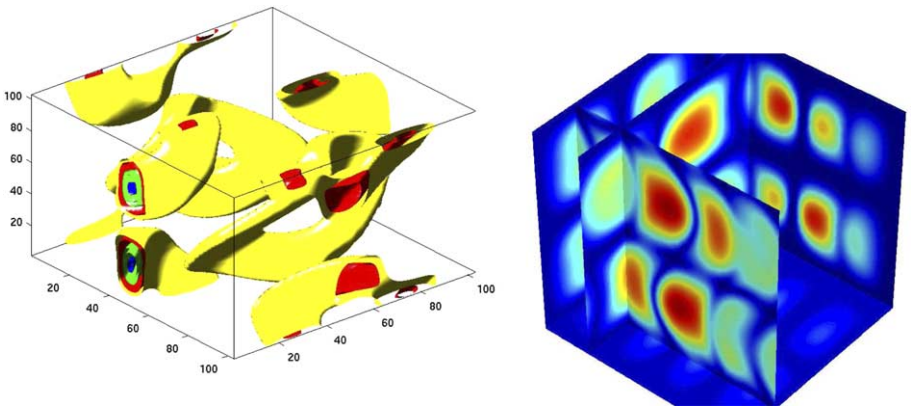

Fig. 13. (Left) Mass density isosurfaces for the three-dimensional Orszag–Tang problem at time $t = 0.5$. (Right) Electric field magnitude contours.

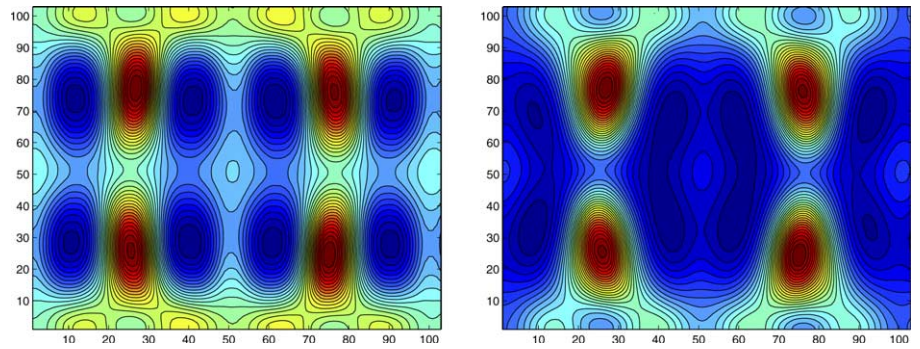

Fig. 14. Contour lines of the mass density (left) and the energy (right) at time $t = 0.5$ in the plane $z = \pi$.

the line $y = z = \pi$ of the energy obtained using the Cartesian dual cell scheme with the aid of the CTCS procedure using 100^3 gridpoints (solid line) and 50^3 gridpoints (dashed line); the dotted line denotes the energy obtained on 50^3 gridpoints using only the diamond dual cell scheme without any divergence treatment. As can be seen in Fig. 15(right), even if we do not apply the CTCS procedure, the numerical results we obtain are still reasonable, and the maximum of the absolute value of $\nabla \cdot \mathbf{B}$ we observe (for this exper-

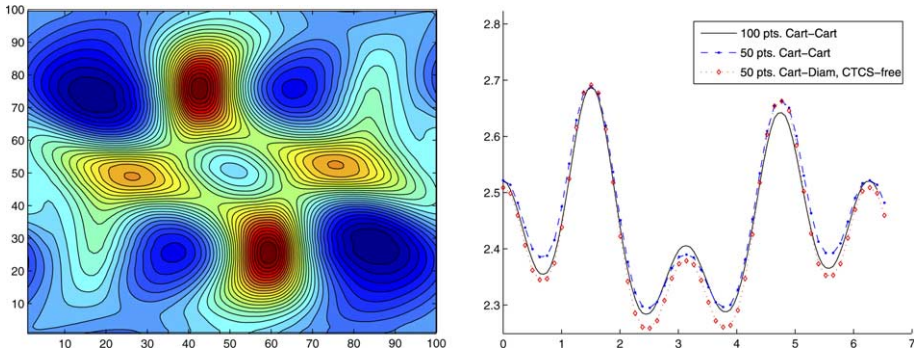

Fig. 15. (Left) Contour lines of the mass density in the plane $z = \pi/2$. (Right) Plots along the line $y = z = \pi/2$ of the energy obtained with (solid line and dashed line) or without (dotted line) the aid of the CTCS procedure.

iment) is about 3.124×10^{-1}. Comparing the dotted line with the dashed line, we find that the effect of the divergence treatment seems to be more necessary in the neighborhood of local extremas.

5.4. Shock–cloud interaction problem

We now consider a three-dimensional adaptation of the classical 2D MHD shock–cloud interaction problem previously considered in several papers [10,24,27,20]. The computational domain $(x, y, z) \in [0, 1]^3$ is uniformly discretized using 100^3 gridpoints. Two constant states $U_l = [3.86859, 11.2536, 0, 0, 167.345, 0, 2.1826182, -2.1826182]$ and $U_r = [1, 0, 0, 0, 1, 0, 0.56418958, 0.56418958]$ are separated by the plane $x = 0.05$; here $U = (\rho, u_x, u_y, u_z, p, B_x, B_y, B_z)$. A 10 times denser spherical cloud centered at (0.25, 0.5, 0.5) with a radius $r = 0.15$ is in hydrostatic equilibrium with the surrounding state. The profile of the initial mass density is shown in Fig. 16(left).

The numerical solution is computed at time $t = 0.06$ using the Cartesian dual cell scheme along with its corresponding CTCS divergence treatment; the maximum absolute value of the divergence observed remains within the 10^{-12} values. An equivalent variant of this three-dimensional problem is considered in [27]. Fig. 16 (right) shows several sections of the contour surfaces (“slides”) of the logarithm of the mass density and also shows(cone plot) the magnitude of the magnetic field. Fig. 17 shows several contour lines of the logarithm of the mass density (left), and several isosurfaces for the energy (right).

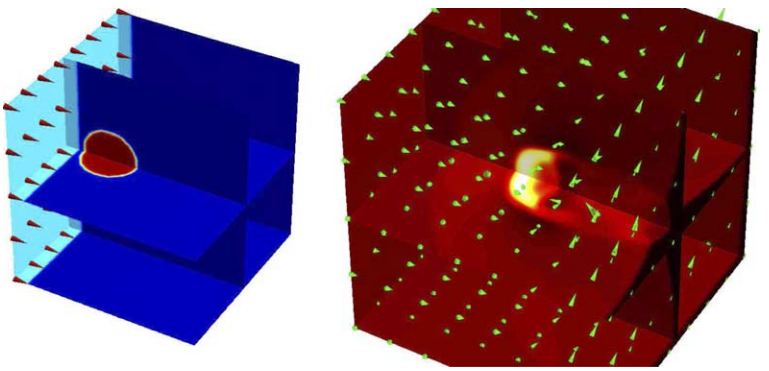

Fig. 16. (Left) Initial mass density profile for the three-dimensional shock–cloud interaction problem; we also see the velocity field magnitude as a cone plot. (Right) several slides illustrating the contours of the logarithm of the mass density; the cone plot represents the magnetic field magnitude.

Fig. 18 shows several plots along the x-axis of the mass density using 60^3, 100^3, and 150^3 gridpoints, respectively. We have compared the results obtained using the MC-θ limiter, for $\theta = 1.5$ and 2 (for the case of 60^3 gridpoints). As it was previously observed for central schemes in the literature, for a given problem, the choice of the limiter may lead to significant improvements of the numerical results; however there is no general rule for this choice, so that one should generally investigate several limiters for best results. The mass density profile obtained using 150 points in the x-direction (shown in Fig. 18) is very similar to the reference solution presented in [27], which was obtained using 200 gridpoints, thus confirming the efficiency of the method.

We observe here that even if we do not apply our CTCS divergence treatment, the base schemes do not become unstable, and may even, in some cases, produce reasonable results. Fig. 19(a) shows the mass density for the shock–cloud interaction problem obtained using the diamond dual cell scheme (on 60^3 gridpoints) without any divergence treatment (dotted plot); the reference solution (solid line) is obtained with the aid of the CTCS divergence treatment on 150^3 gridpoints. Fig. 19(b) shows the same comparison for the energy. We observe that when we do not apply the CTCS procedure, the divergence of the magnetic field is not negligible (Fig. 19(c) $\nabla \cdot \mathbf{B}$ along the line $y = z = 0.5$ and Fig. 19(e) $\nabla \cdot \mathbf{B}$ in the plane $z = 0.5$; Fig. 19(d) and (f) show the corresponding result when the CTCS procedure is applied). Moreover, we find

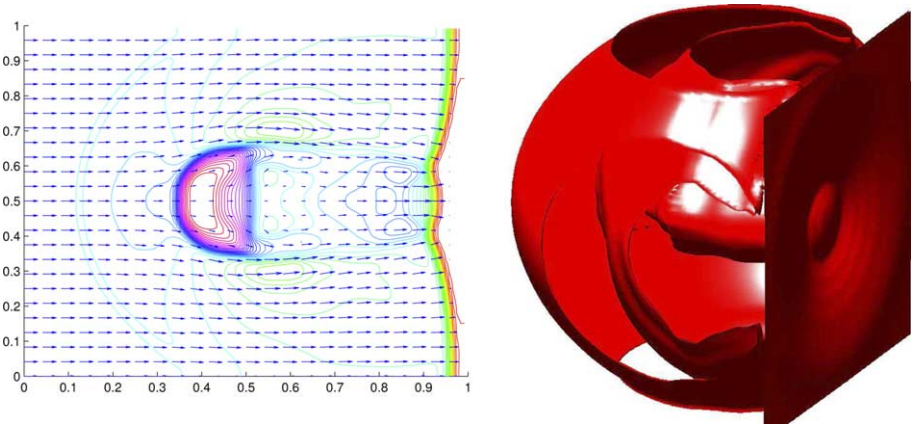

Fig. 17. (Left) Several contour lines of the mass density logarithm at time $t = 0.06$ for the three-dimensional shock–cloud interaction. (Right) Several isosurfaces for the energy.

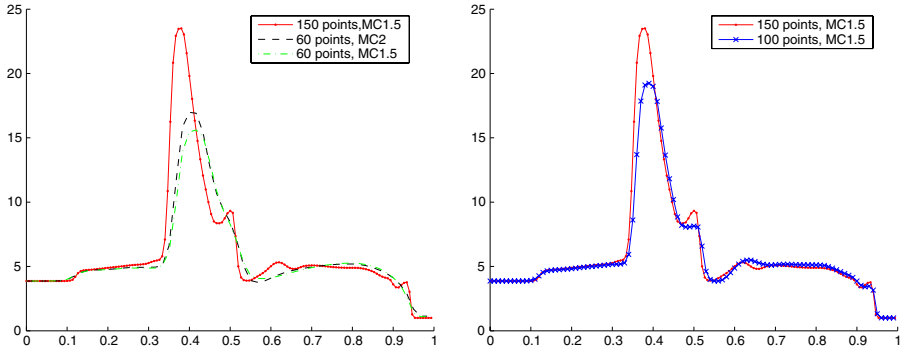

Fig. 18. Several plots of the mass density of the shock–cloud interaction problem along the line $y = 0.5$ in the plane $z = 0.5$ obtained using the MC-1.5 limiter (right) and the MC-1.5 and MC-2 limiters (left).

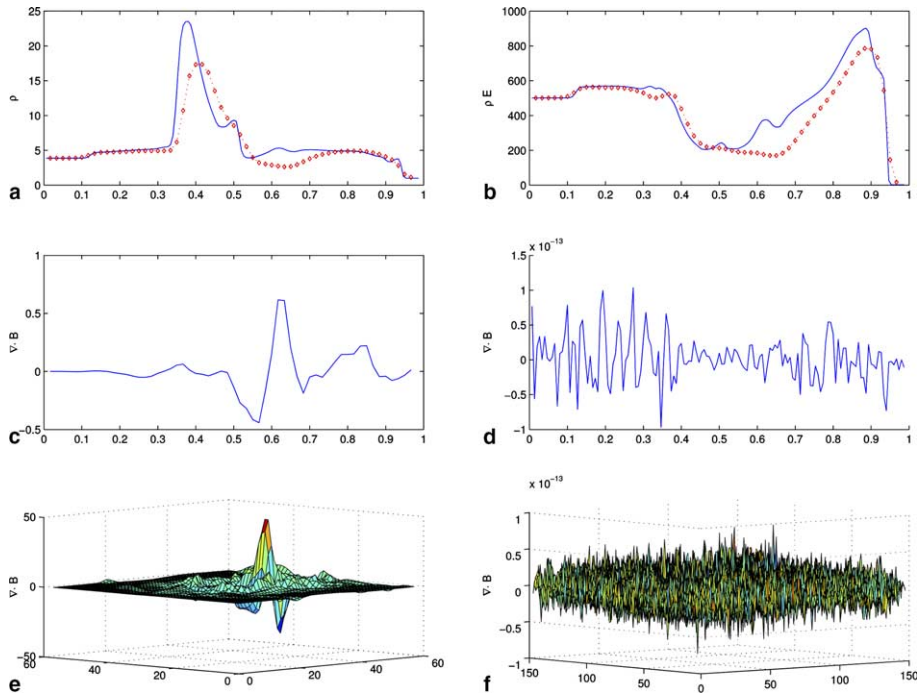

Fig. 19. Shock–cloud interaction problem: (a) plot of the mass density along the line $y = z = 0.5$, $0 \leqslant x \leqslant 1$ obtained using the base scheme with the CTCS (150 points, solid line) and without any divergence treatment (60 points, dotted line); same comparison for the energy (b).

(Fig. 19(a) and (b)) that deviations from the reference solution are important, quantitatively, when the divergence values are non-negligible, and particularly so, qualitatively (wrong sense of variation, locally) where the divergence values are relatively large. We mention here that the solution obtained without the aid of the CTCS treatment is physically inadmissible but allows us to appreciate the base scheme which did not crash while several other numerical methods broke down.

6. Conclusion

In this paper, we have presented three-dimensional, second-order accurate, central numerical methods for solving systems of hyperbolic equations. To avoid the resolution of the Riemann problems at the cell interfaces, the numerical solution alternates between an original and a staggered grid; we have considered two possibilities for the dual cells of the staggered grid (Cartesian or diamond-shaped), while those of the original grid are Cartesian cells. The fact that the numerical scheme does not require any characteristic field decomposition, will clearly reduce computing times as compared with methods based on exact [13] or approximate [9,19] Riemann problem solvers. We have adapted these central methods to ideal magnetohydrodynamics and solved some three-dimensional ideal MHD problems.

- To satisfy the divergence-free magnetic field constraint, we have constructed a new three-dimensional CTCS method (based on the constrained transport approach) that treats, after each time step, the magnetic field components obtained using the numerical base scheme. The CTCS procedure applies to both

Cartesian dual cell and diamond dual cell schemes and is second-order accurate, and thus preserves the second-order accuracy of the base scheme. The divergence of the magnetic field for the problems we considered in this paper remains of the order of 10^{-12}, which is smaller than the error introduced by the computation of the divergence with the help of central differences. Both the numerical base scheme and the CTCS procedure are easy to implement on a single processor computer or a multi-processor cluster.

- For the ideal MHD problems considered in this paper, both numerical base schemes can reach the final time (and sometimes even generate reasonable results) without producing instabilities, without the application of the CTCS procedure, contrary to many other numerical schemes that often break down in the early stages of the computations. However the base schemes (alone) fail to produce a divergence-free magnetic field in the numerical solution. For this reason, as a general rule, the CTCS divergence treatment should be applied.
- As it is well known (for central schemes), one should consider several choices of limiters for a given problem. Van Leer's MC-θ limiter usually leads to good results. For the numerical experiments we considered in this paper, we observed that the diamond dual cell scheme leads to a slightly better capture of discontinuities, as compared to the Cartesian dual cell scheme, but it is clearly more complicated and more time-consuming since one should compute three sets of solutions on the dual cells at each odd time step (on the cells $D_{i+1/2,j,k}$, $D_{i,j+1/2,k}$, and $D_{i,j,k+1/2}$). Regarding the computing time of each approach, many parameters may be considered such as the computing equipments and the programming approaches and techniques. However, in our numerical three-dimensional experiments we have observed that the Cartesian dual cell scheme may save about 40–45% of the computing time as compared to the diamond dual cell scheme, which is a considerable amount of time in view of the very large computing-times prevailing for three-dimensional MHD.

The numerical results we obtained using both base schemes compare very well to one another and are in very good agreement with others appearing in the literature.

Appendix A

For the sake of completeness, we shall describe here the CTCS method in the case of Cartesian dual cells. We suppose that the solution is given on the original grid at time t^n and the magnetic field satisfies the divergence-free property, (i.e. Eq. (18) is true). Let $\mathbf{B}^n_{i,j,k} = (B^{n,x}, B^{n,y}, B^{n,z})_{i,j,k}$ denote the magnetic field and $\mathbf{E}^{n+1/2}_{i+1/2,j+1/2,k+1/2} = (\Omega^x, \Omega^y, \Omega^z)_{i+1/2,j+1/2,k+1/2}$ the electric field at time t^n and $t^{n+1/2}$, respectively. We denote by $\mathbf{B}^*_{i+1/2,j+1/2,k+1/2}$ the magnetic field obtained using the numerical base scheme and computed on the Cartesian dual grid; the CTCS-treated, divergence-free, magnetic field will be denoted by $\mathbf{B}^{n+1}_{i+1/2,j+1/2,k+1/2}$. We first compute the electric field at time $t^{n+1/2}$ on the staggered dual cells as follows:

$$\begin{aligned}\mathbf{E}^{n+1/2}_{i+1/2,j+1/2,k+1/2} &= -(\mathbf{v}\times\mathbf{B})^{n+1/2}_{i+1/2,j+1/2,k+1/2}\\ &= -\frac{1}{2}\left[(\mathbf{v}^{n+1}\times\mathbf{B}^*)_{i+1/2,j+1/2,k+1/2} + \frac{1}{8}\left\{(\mathbf{v}\times\mathbf{B})^n_{i,j,k} + (\mathbf{v}\times\mathbf{B})^n_{i+1,j,k} + (\mathbf{v}\times\mathbf{B})^n_{i+1,j+1,k}\right.\right.\\ &\quad \left.\left. + (\mathbf{v}\times\mathbf{B})^n_{i,j+1,k} + (\mathbf{v}\times\mathbf{B})^n_{i,j,k+1} + (\mathbf{v}\times\mathbf{B})^n_{i+1,j,k+1} + (\mathbf{v}\times\mathbf{B})^n_{i+1,j+1,k+1} + (\mathbf{v}\times\mathbf{B})^n_{i,j+1,k+1}\right\}\right].\end{aligned} \tag{28}$$

This particular discretization of the electric field preserves the second-order accuracy with respect to time of the base scheme. Next, we discretize the induction equation (20) on the staggered grid using central differences and update the magnetic field components at time t^{n+1} as follows:

$$B^{n+1,x}_{i+1/2,j+1/2,k+1/2} = \frac{1}{8}(B^{n,x}_{i,j,k} + B^{n,x}_{i+1,j,k} + B^{n,x}_{i+1,j+1,k} + B^{n,x}_{i,j+1,k} + B^{n,x}_{i,j,k+1} + B^{n,x}_{i+1,j,k+1} + B^{n,x}_{i+1,j+1,k+1} + B^{n,x}_{i,j+1,k+1}) - \Delta t \frac{\Omega^{n+1/2,z}_{i+1/2,j+3/2,k+1/2} - \Omega^{n+1/2,z}_{i+1/2,j-1/2,k+1/2}}{2\Delta y} + \Delta t \frac{\Omega^{n+1/2,y}_{i+1/2,j+1/2,k+3/2} - \Omega^{n+1/2,y}_{i+1/2,j+1/2,k-1/2}}{2\Delta z}, \quad (29)$$

$$B^{n+1,y}_{i+1/2,j+1/2,k+1/2} = \frac{1}{8}(B^{n,y}_{i,j,k} + B^{n,y}_{i+1,j,k} + B^{n,y}_{i+1,j+1,k} + B^{n,y}_{i,j+1,k} + B^{n,y}_{i,j,k+1} + B^{n,y}_{i+1,j,k+1} + B^{n,y}_{i+1,j+1,k+1} + B^{n,y}_{i,j+1,k+1}) - \Delta t \frac{\Omega^{n+1/2,x}_{i+1/2,j+1/2,k+3/2} - \Omega^{n+1/2,x}_{i+1/2,j+1/2,k-1/2}}{2\Delta z} + \Delta t \frac{\Omega^{n+1/2,z}_{i+3/2,j+1/2,k+1/2} - \Omega^{n+1/2,z}_{i-1/2,j+1/2,k+1/2}}{2\Delta x}, \quad (30)$$

$$B^{n+1,z}_{i+1/2,j+1/2,k+1/2} = \frac{1}{8}(B^{n,z}_{i,j,k} + B^{n,z}_{i+1,j,k} + B^{n,z}_{i+1,j+1,k} + B^{n,z}_{i,j+1,k} + B^{n,z}_{i,j,k+1} + B^{n,z}_{i+1,j,k+1} + B^{n,z}_{i+1,j+1,k+1} + B^{n,z}_{i,j+1,k+1}) - \Delta t \frac{\Omega^{n+1/2,y}_{i+3/2,j+1/2,k+1/2} - \Omega^{n+1/2,y}_{i-1/2,j+1/2,k+1/2}}{2\Delta x} + \Delta t \frac{\Omega^{n+1/2,x}_{i+1/2,j+3/2,k+1/2} - \Omega^{n+1/2,x}_{i+1/2,j-1/2,k+1/2}}{2\Delta y}. \quad (31)$$

With this particular symmetric discretization of the induction equation and the special choice for the electric field at intermediate time $t^{n+1/2}$, we can prove that:

$$\nabla \cdot \mathbf{B}^{n+1}_{i+1/2,j+1/2,k+1/2} = \frac{1}{8}\{\nabla \cdot \mathbf{B}^{n}_{i,j,k} + \nabla \cdot \mathbf{B}^{n}_{i+1,j,k} + \nabla \cdot \mathbf{B}^{n}_{i+1,j+1,k} + \nabla \cdot \mathbf{B}^{n}_{i,j+1,k} + \nabla \cdot \mathbf{B}^{n}_{i,j,k+1} + \nabla \cdot \mathbf{B}^{n}_{i+1,j,k+1} + \nabla \cdot \mathbf{B}^{n}_{i+1,j+1,k+1} + \nabla \cdot \mathbf{B}^{n}_{i,j+1,k+1}\}. \quad (32)$$

Eq. (32) shows that if the magnetic field at time t^n is divergence-free, the CTCS-updated magnetic field will also satisfy the physical constraint. Let us observe here that this CTCS approach can be specialized to the two-dimensional case for Cartesian dual cells by omitting the differentiation with respect to z in Eqs. (29),(30) and by replacing all pairs of terms such as $B^{n,x}_{i,j,k}$ and $B^{n,x}_{i,j,k+1}$ by $B^{n,x}_{i,j}$ in Eqs. (28)–(30). Note that in the two-dimensional case the z component of the magnetic field does not need to be treated as it no longer contributes to the divergence.

References

[1] P. Arminjon, M.C. Viallon, Généralisation du schéma de Nessayahu–Tadmor pour une équation hyperbolique à deux dimensions d'espace, C.R. Acad. Sci. Paris, 320(I) (1995) 85–88.

[2] P. Arminjon, D. Stanescu, M.C. Viallon, A two-dimensional finite volume extension of the Lax–Friedrichs and Nessyahu–Tadmor schemes for compressible flows, in: M. Hafez, K. Oshima (Eds.), Proc. of the 6th Int. Symp. on Comp. Fluid Dynamics, vol. IV, 1995, pp. 7–14.

[3] P. Arminjon, M.C. Viallon, A. Madrane, A finite volume extension of the Lax–Friedrichs and Nessyahu–Tadmor schemes for conservation laws on unstructured grids, revised version with numerical applications, Int. J. Comp. Fluid Dynamics 9 (1) (1997) 1–22.

[4] P. Arminjon, M.C. Viallon, Convergence of a finite volume extension of the Nessyahu–Tadmor scheme on unstructured grids for a two-dimensional linear hyperbolic equation, SIAM J. Numer. Anal. 36 (3) (1999) 738–771.

[5] P. Arminjon, R. Touma, Central finite volume methods with constrained transport divergence treatment for ideal MHD, J. Comput. Phys. 204 (2005) 737–759.

[6] J. Balbas, E. Tadmor, C.C. Wu, Non-oscillatory central schemes for one- and two-dimensional MHD equations, J. Comput. Phys. 201 (2004) 261–285.

[7] D.S. Balsara, D.S. Spicer, A staggered mesh algorithm using high order Godunov fluxes to ensure solenoidal magnetic fields in magnetohydrodynamic simulations, J. Comput. Phys. 149 (1999) 270.

[8] J.U. Brackbill, D.C. Barnes, The effect of nonzero $\nabla \cdot \mathbf{B}$ on the numerical solution of the magnetohydrodynamic equations, J. Comput. Phys. 35 (1980) 426.

[9] M. Brio, C.C. Wu, An upwind differencing scheme for the equations of ideal magnetohydrodynamics, J. Comput. Phys. 75 (2) (1988) 400–422.

[10] W. Dai, P.R. Woodward, A simple finite difference scheme for multidimensional magnetohydrodynamical equations, J. Comput. Phys. 142 (1998) 331–369.

[11] P. Londrillo, L. Del Zanna, High-order upwind schemes for multidimensional magnetohydrodynamics, Astrophys. J. 530 (2000) 508–524.
[12] C.R. Evans, J.F. Hawley, Simulation of magnetohydrodynamic flows: A constrained transport method, Astrophys. J. 332 (1988) 659.
[13] S.K. Godunov, A difference scheme for numerical computation of discontinuous solutions of equations of fluid dynamics, Math. Sb. 47 (89) (1959) 271–306.
[14] G. Jiang, E. Tadmor, Non-oscillatory central schemes for multidimensional hyperbolic conservation laws, SIAM J. Sci. Comput. 19 (1998) 1892–1917.
[15] H. Nessyahu, E. Tadmor, Non-oscillatory central differencing for hyperbolic conservation laws, J. Comput. Phys. 87 (2) (1990) 408–463.
[16] C. Nodes, G.T. Gritschneder, H. Lesch, Radio emission and particle acceleration in plerionic supernova remnants, Astronom. Astrophys. 423 (2004) 13–19.
[17] K.G. Powell, P.L. Roe, T.J. Linde, T.I. Gombosi, D.L. De Zeeuw, A solution-adaptive upwind scheme for ideal magnetohydrodynamics, J. Comput. Phys. 154 (1999) 284.
[18] K.G. Powell, P.L. Roe, R.S. Myong, T. Gombosi, D. De Zeeuw, An upwind scheme for magnetohydrodynamics, AIAA Paper 95-1704-CP, 1995.
[19] K.G. Powell, An approximate Riemann solver for magnetohydrodynamics (that works in more than one dimension), NASA ICASE report No. 94-24, Langley, VA, 1994.
[20] J. Rossmanith, A wave propagation method with constrained transport for ideal and shallow water magnetohydrodynamics, Ph.D. Thesis, Department of Mathematics, University of Washington, 2002.
[21] D. Ryu, F. Miniati, T.W. Jones, A. Frank, A divergence-free upwind code for multi-dimensional magnetohydrodynamic flows, Astrophys. J. 509 (1998) 244.
[22] D. Ryu, T.W. Jones, Numerical magnetohydrodynamics in astrophysics: Algorithm and tests for one-dimensional flow, Astrophys. J. 442 (1995) 228.
[23] G.A. Sod, A survey of finite-difference methods for systems of nonlinear conservation laws, J. Comput. Phys. 27 (1978) 1–31.
[24] G. Tóth, The $\nabla \cdot \mathbf{B} = 0$ constraint in shock-capturing magnetohydrodynamics codes, J. Comput. Phys. 161 (2000) 605–652.
[25] G. Tóth, D. Odstrčil, Comparison of some flux corrected transport and total variation diminishing numerical schemes for hydrodynamic and magnetohydrodynamic problems, J. Comput. Phys. 128 (1996) 82.
[26] B. van Leer, Towards the ultimate conservative difference scheme V. A second-order sequel to Godunov's method, J. Comput. Phys. 32 (1979) 101–136.
[27] U. Ziegler, A central-constrained transport scheme for ideal magnetohydrodynamics, J. Comput. Phys. 192 (2004) 393–416.